(53) Cowie, J. M. G.; Bywater, S.; Worsfold, D. J. *Polymer* **1967**, *8*, 105.
(54) Noda, I.; Mizutani, K.; Kato, T.; Fujimoto, T.; Nagasawa, M. *Macromolecules* **1970**, *3*, 787.
(55) McCormick, H. W. *J. Polym. Sci.* **1959**, *41*, 327.
(56) Altares, T.; Wyman, D. P.; Allen, V. R. *J. Polym. Sci., Part A* **1964**, *2*, 4533.
(57) Bianchi, U.; Dalpiaz, M.; Patrone, E. *Makromol. Chem.* **1964**, *80*, 112.
(58) Fox, T. G.; Kinsinger, J. B.; Mason, H. F.; Schuele, E. M. *Polymer* **1962**, *3*, 71.
(59) George, A.; Wilson, W. W.; Mays, J. W.; Lindner, J. S., to be submitted for publication.
(60) Muthukumar, M.; Freed, K. F. *Macromolecules* **1977**, *10*, 899.
(61) One could question the validity of using average values in Tables III and IV. It is our opinion, however, that considering the possible experimental errors the initial use of average values is a reasonable first approximation. Large standard deviations would therefore imply either experimental errors or trends in the data.
(62) Simionescu, C. I.; Simionescu, B. C.; Neamtu, I.; Ioan, S. *Polymer* **1987**, *28*, 165. Simionescu, B. C.; Ioan, S.; Simionescu, C. I. *J. Polym. Sci., Polym. Phys. Ed.* **1987**, *25*, 829.
(63) Appelt, B.; Meyerhoff, G. *Macromolecules* **1980**, *13*, 657.
(64) Mays, J. W.; Hadjichristidis, N.; Fetters, L. J. *Macromolecules* **1985**, *18*, 2231.
(65) Schmidt, M.; Burchard, W. *Macromolecules* **1981**, *14*, 210.
(66) Freed, K. F. *Renormalization Group Theory of Macromolecules*; Wiley: New York, 1987, Chapter 10.
(67) Rey, A.; Freire, J.; Garcia de la Torre, J. *Macromolecules* **1987**, *20*, 342.
(68) Wang, S. Q.; Douglas, J. F.; Freed, K. F. *Macromolecules* **1985**, *18*, 2469.
(69) Wang, S. Q.; Douglas, J. F.; Freed, K. F. *J. Chem. Phys.* **1985**, *85*, 3674.
(70) As a reviewer pointed out, Ferry and co-workers at Wisconsin have also detected deviations from the least-draining limit (via viscoelastic measurements) for PS, PαMS, and other flexible polymers at high molecular weights in good solvents. See for example: Osaki, K.; Schrag, J. L.; Ferry, J. D. *Macromolecules* **1972**, *5*, 144.
(71) Zimm, B. H. *Macromolecules* **1980**, *13*, 592.
(72) Huber, K.; Burchard, W.; Akcasu, A. Z. *Macromolecules* **1985**, *18*, 2743.
(73) LeGuillou, J. C.; Zinn-Justin, J. *Phys. Rev. Lett.* **1977**, *39*, 95.
(74) Adam, M.; Delsanti, M. *Macromolecules* **1977**, *10*, 1229.

Solution Properties of Exocellular Microbial Polysaccharides. 3. Light Scattering from Gellan and from the Exocellular Polysaccharide of *Rhizobium trifolii* (Strain TA-1) in the Ordered State

M. Dentini,† T. Coviello,† W. Burchard,*,‡ and V. Crescenzi†

Dipartimento di Chimica, Università di Roma, "La Sapienza", 00185 Rome, Italy, and Institut für Makromolekulare Chemie, Universität Freiburg, 7800 Freiburg, FRG.
Received December 10, 1987; Revised Manuscript Received April 15, 1988

ABSTRACT: Exocellular microbial polysaccharides (EPS) from *Rhizobium trifolii* strain TA-1 (TA-1-EPS) and from *Pseudomonas elodea* (Gellan) have been studied in dilute aqueous salt solutions by static and dynamic light scattering (LS) under conditions where the two polysaccharides are in the ordered (helical) state. The two polymers show pronounced chain rigidity. Their LS behavior has been evaluated from static and dynamic Zimm plots, i.e., Kc/R_θ versus q^2 and $D_{app}(q) = \Gamma/q^2$ versus q^2, and from Holtzer plots, i.e., $qR_\theta/(Kc)$ versus $q = (4\pi/\lambda) \sin \theta/2$. From the two types of Zimm plots the common molecular parameters, i.e., molecular weight M_w, radius of gyration $R_g = \langle S^2 \rangle_z^{1/2}$, and translational diffusion coefficient D_Z, were obtained. The Holtzer plots exhibit a clear asymptotic rod behavior. The value of the asymptotic plateau at large q gives the linear mass density (=mass per unit length) $M_L = M/L$. Comparison of the experimentally observed data to those calculated for a single-stranded helix allowed determination of the number of laterally associated strands which were found to be $n = 3.02 \pm 0.07$ and $n = 1.85 \pm 0.02$ for TA-1-EPS and Gellan, respectively. The Kuhn segment lengths could be estimated from the ratio of the heights of the maximum and asymptotic plateau in the Holtzer plot and were found to be $l_k = 152$ nm for TA-1-EPS and $l_k = 322$ nm for Gellan. These large values lie in the same range as the Kuhn segment lengths for other microbial polysaccharides. The observed angular dependence was checked with the predictions by Koyama for stiff chains and by Benoit et al. for flexible chains with large excluded volume. A good agreement was found with Koyama's prediction whereas application of the relationship for chains with large excluded-volume effect produces strong deviations. The large chain stiffness is confirmed by the value of the ρ-parameter R_g/R_h, where R_h is the hydrodynamically effective radius.

Introduction

In recent years a number of exocellular microbial polysaccharides (ESP) have aroused keen interest because of their unique solution and gelling properties.[1] In many instances, these properties have already opened avenues to the industrial utilization of such biopolymers,[2] while new species continue to appear as additional, interesting candidates for both basic and applied researches.[3]

A feature which seems to be in common to all EPSs so far studied is that in very dilute aqueous solution more or less disordered chains (probably, but not necessarily, single chains) would prevail. However, upon increasing polymer concentration and with added salt the EPS chains almost invariably undergo conformational disorder–order transitions. Because of the often highly cooperative character, this transition can be easily monitored by common physical–chemical techniques, e.g., chiroptical, calometric, and viscometric techniques.[4,5]

None of these experimental approaches can give, however, an unambigious answer to the central question of the final ordered conformation for the chains in each case (e.g., single helix or multiple-stranded helix). Kinetic measurements can be of valuable help in elucidating this important point.[6,7] In the context, radiation scattering (i.e., small-angle X-ray, small-angle neutron, and laser light scattering) appears quite naturally the most appropriate

* Author to whom correspondence should be addressed.
† Università di Roma.
‡ Universität Freiburg.

0024-9297/88/2221-3312$01.50/0

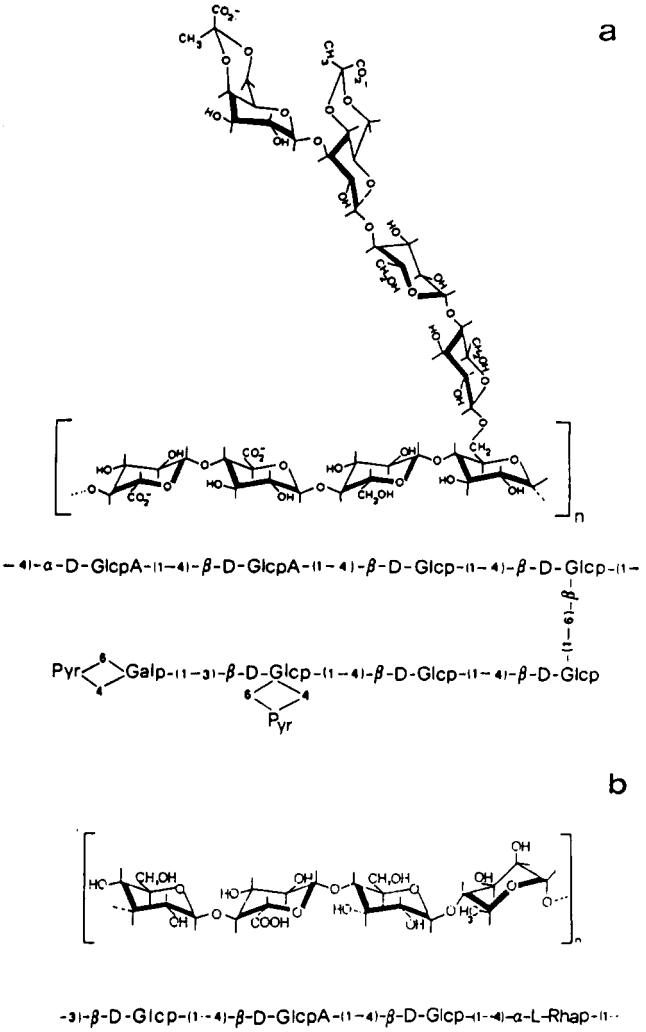

Figure 1. Chemical repeating unit for (a) the exo polysaccharide (EPS) from *Rhizobium trifolii*, strain TA1 (TA1-EPS), and (b) Gellan.

approach, at least in principle, provided the occurrence of unspecific chain aggregation can be avoided.

With the present investigation we continue our studies on the conformation of microbial polysaccharides in dilute salt solution, which was started with a detailed examination of native xanthan and chemically modified xanthans.[8-10] The applied technique, a combination of static and dynamic light scattering, makes it possible to determine the chain stiffness and the number of strands building up the ordered conformational states.

The two polysaccharides of this study are (1) the EPS product by *Rhizobium trifolii* strain TA-1 (hereafter indicated as TA-1-EPS) and (2) the EPS from *Pseudomonas elodea*, commonly named Gellan. The repeating units of TA-1-EPS and Gellan are depicted in Figure 1. The salt-induced, highly cooperative conformational transition of these two anionic bacterial polysaccharides in dilute aqueous solution has been already characterized in a rather detailed fashin in terms of associated energy, optical activity, and intrinsic viscosity changes.[4,5,11]

Experimental Section

Sample Preparation. The origin and purification of the exocellular polysaccharide from *Pseudomonas elodea*, deacetylated sample (Gellan), have been reported elsewhere.[4,5] The exocellular polysaccharide (EPS) extracted from *Rhizobium trifolii*, strain TA-1, has been isolated at the Department of Microbiology of the University of Wageningen, The Netherlands, by Dr. Zevenhuizen.[12] Further purification was performed as follows: The polysaccharide was dissolved in water and the solution was dialyzed over night against NaCl and then dialyzed exhaustively against double-distilled water, until the absence of an excess of salt was indicated by conductivity measurements. The sample solution was then neutralized, filtered, and freeze-dried. The equivalent weight of the TA-1-EPS sample, determined on the basis of potentiometric titration data, was found to be 396 in agreement with structural data.[12]

Table I
Molecular Weight M_w; Experimental and Calculated Radii of Gyration[a] R_g(exptl), R_g(calcd, poly), R_g(calcd, mono); Second Virial Coefficient A_2; Calculated and Measured Linear Mass Density M_L(single) and M_L(exptl); Ratio of Measured and Calculated Linear Mass Density; Ratio of Maximum and Asymptote from the Holtzer Plot; Contour Length L_w; Number of Kuhn Length N_k;[a] and Length of Kuhn Segment l_k[a]

parameter	TA1-EPS	Gellan	xanthan	PBLG
$M_w \times 10^{-6}$, Da	1.29	0.434	2.94	0.560
R_g(exptl), nm	127	159	290	101
R_g(calcd, poly), nm	113 ± 10	153 ± 17	298	
R_g(calcd, mono), nm	(100 ± 2)[b]	(134 ± 14)[b]	(263)[b]	
$A_2 \times 10^4$, cm³ mol/g²	6.90	22.0	4.94	2.50
M_L(single), Da/nm	826	395	899	
M_L(exptl), Da/nm	2490 ± 60	710 ± 10	1830 ± 80	
M_L(exptl)/M_L(single)	3.02 ± 0.07	1.80 ± 0.02	2.00 ± 0.10	
max/asymptote	1.30 ± 0.03	1.12 ± 0.01	1.52 ± 0.07	
L_w, nm	517 ± 10	611 ± 9	1609 ± 70	392
N_k(poly)	4.2 ± 0.3	3.0 ± 0.2	6.3 ± 0.6	2.8
N_k(mono)	2.8 ± 0.3	1.7 ± 0.2	(4.6 ± 0.6)	
l_k(poly), nm	123 ± 6	204 ± 14	255 ± 15	140
l_k(mono), nm	185 ± 15	359 ± 6	(350 ± 50)[b]	
d, nm[c]	1.89	1.01	1.62	

[a] For polydisperse and monodisperse chains. [b] The parentheses indicates that these data can be excluded from the position of the maximum in the Holtzer plot. [c] According to eq 8.

Preparation of Solutions for Light Scattering. Stock solutions for light scattering were prepared by dissolving the polymer in the proper concentration of NaCl and then dialyzing against aqueous solutions of the same salt concentration for 5 days in a special cell at constant volume. The dilutions were made with the dialyzed solvent, and the solutions of suitable concentration (0.2×10^{-3} to 1×10^{-3} g/cm³) were filtered trough 0.45-μm Millipore, sterilized, one-way filters, directly into the light scattering cells.

Light Scattering. Static and dynamic light scattering measurements were carried out simultaneously in the angular range 30–140° at 25 °C with the blue line (λ_0 = 488 nm) of an Ar ion laser (Spectra Physics, Model Ar 165-06). Details of the instrument and on data evaluation are given in ref 13.

Refractive Index Increment. The values of the refractive index increment of the two polysaccharides were evaluated with a Phoenix 60 differential refractometer at λ_0 = 488 nm. Values of 0.145 and 0.156 cm³/g were found for TA1-EPS in 0.1 M NaCl and for Gellan in 0.075 M TMACl (tetramethylammonium chloride), respectively.

Results

TA-1-EPS Polysaccharide. 1. Static Light Scattering. Static and dynamic light scattering experiments have been performed simultaneously at 25 °C in a wide concentration range up to 8.6×10^{-3} g/cm³ in aqueous 0.1 m NaCl solutions. According to the optical rotation measurements, the polysaccharide is in the ordered state at that ionic strength. Here we confine ourselves to the dilute concentration regime. Figure 2 shows the typical Zimm plot for the five lowest concentrations (2.2×10^{-4} to 1.1×10^{-3} g/cm³). The angular dependence shows a slight downward curvature, which is characteristic of stiff chains.[14,15] The very strong concentration dependence indicates the aqueous salt solution as a thermodynamically good solvent. The molecular weight M_w, radius of gyration $R_g = \langle S^2 \rangle_z^{1/2}$, and second virial coefficient A_2 are given in Table I.

For a better characterization of the structure the same data were plotted in Figure 3 as $qR_\theta/\pi Kc$ against $q\langle S^2 \rangle_c^{1/2}$,

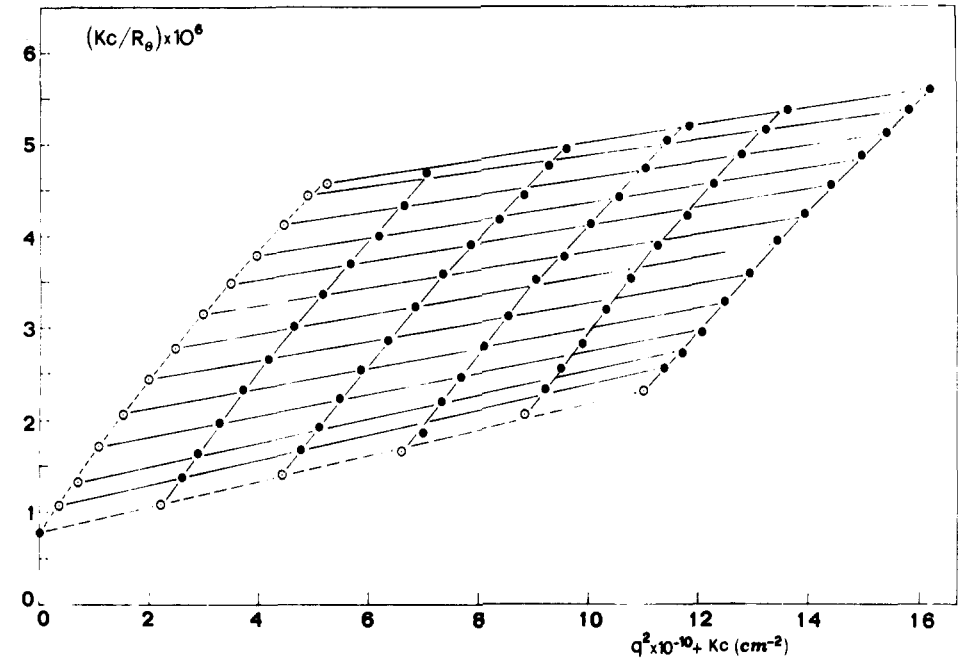

Figure 2. Zimm plot of the static light scattering measurements from TA-1-EPS in 0.1 M NaCl at 25 °C and concentrations of c = 0.22, 0.44, 0.66, 0.88, and 1.1 × 10^{-3} g/cm^3.

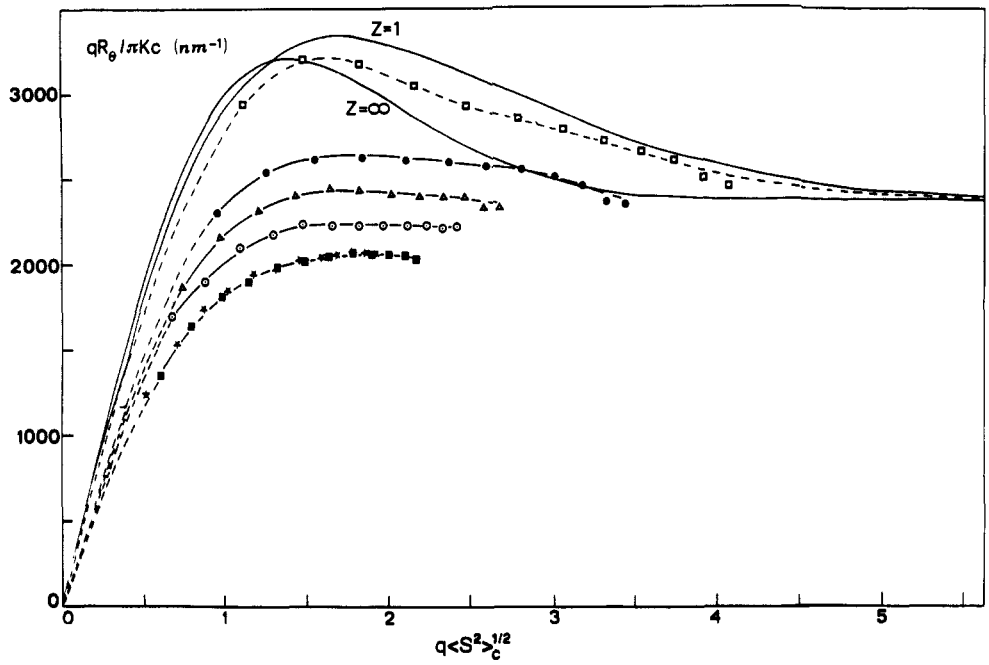

Figure 3. Holtzer plots for the same TA-1-EPS as in Figure 2 in 0.1 M NaCl at 25 °C; lowest curve corresponds to c = 1.1 × 10^{-3} g/cm^3; (□) extrapolated values for c = 0; full lines were calculated according to the Koyama theory with the set of parameters as given in Table I.

where R_θ is the Rayleigh ratio, K the optical contrast factor, and $\langle S^2\rangle_c^{1/2}$ the apparent radius of gyration at the concentration c. This plot, named the Holtzer plot,[16,17] is most instructive for the interpretation of semiflexible chain molecules as it approaches asymptotically a constant plateau at large q values. This asymptote is indicative of rigid-rod behavior[17] of short chain sections (Kuhn segment lengths). Its value gives the linear mass density M_L

$$qR_\theta/\pi Kc \rightarrow M_L \qquad (1)$$

which represents the mass per unit length of the rod. This value can be calculated for a single-stranded chain by using the repeating unit molecular weight of M_0 = 1554 and the corresponding length of 1.88 nm (assuming the typical (1,4)-glucose unit length in a cellulose backbone), which gives M_L(single strand) = 827 Da/nm (Da = dalton). The experimental value of M_L is difficult to estimate from Figure 3 since the asymptote has not been reached. However, from the extrapolated curve and from the second lowest concentration, it becomes clear that the asymptotic value of M_L(exptl) must lie in between 2430 and 2545 Da/nm. The ratio of M_L(exptl)/M_L(single) gives the number of laterally interacting strands of the ordered TA-1-EPS conformation in solution (0.1 M NaCl), which is found to be n(strands) = 3.02 ± 0.07.

The Holtzer plot shows a maximum at low values of q as predicted theoretically by the Koyama theory[18] for semiflexible chains. In a recent paper Schmidt et al.[16] noticed that the ratio of the heights of the maximum to the asymptote is a function of the number of Kuhn seg-

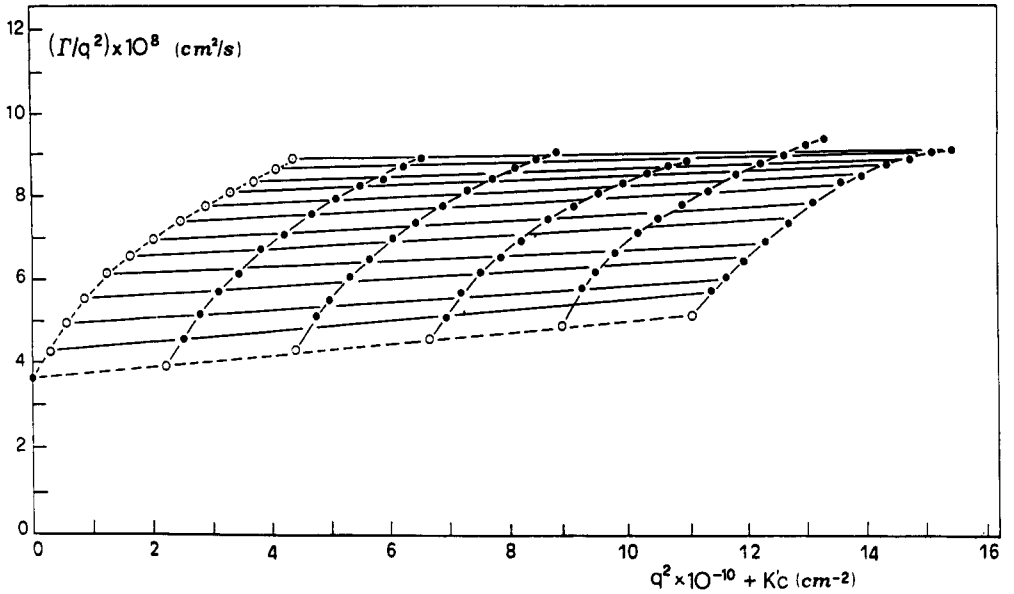

Figure 4. Dynamic Zimm plot of the light scattering measurements from TA-1-EPS in 0.1 M NaCl at 25 °C. Γ is the first cumulant and $q = (4\pi/\lambda) \sin \theta/2)$. The value of $\Gamma/q^2 = D_{app}(q)$ at zero angle gives the translational diffusion coefficient D_c at the concentration c.

ments N_k per chain. The dependence of this ratio as a function of N_k was calculated for polydisperse ($z = 1$, i.e., $M_w/M_n = 2$) and for monodisperse chains ($z = \infty$; i.e.,; $M_w/M_n = 1$). With the experimentally determined ratio of 1.3 ± 0.3 we obtain $N_k = 4.2 \pm 0.3$ and 2.8 ± 0.3 for polydisperse and monodisperse chains, respectively. The contour length L_w is found from the molecular weight M_w and linear mass density M_L according to the equation

$$L_w = M_w/M_L \quad (2)$$

which gives 517 ± 6 nm. Finally the Kuhn segment length is obtained from the relationship

$$l_k = L_w/N_k \quad (3)$$

Inserting the values for L_w and N_k, one obtains $l_k = 123 \pm 6$ nm for the polydisperse and 185 ± 15 for the monodisperse chain.

In principle the polydispersity of the chain can be estimated from the position of the maximum in the Holtzer plot.[16] For the polydisperse chain the maximum should occur at $u = qR_g = 1.73$ ($R_g = \langle S^2 \rangle^{1/2}$), while for the monodisperse one it should occur at $u = 1.4$. The maximum occurs in Figure 3 at 1.6 ± 0.11. This leads to the conclusion that the TA-1-EPS sample has a polydispersity index of approximately $M_w/M_n = 1.6$. All conformational properties that were derived from the Zimm plot are collected in Table I. The obtained data can be cross-checked by calculating the radius of gyration and angular dependence of the scattered light by using the equation of Benoit and Doty[19] and Koyama,[18] respectively. These calculations give radii of gyration of 113 and 100 nm for the polydisperse and monodisperse cases, respectively.

2. Dynamic Light Scattering. From the initial slope of the dynamic light scattering time correlation function (TCF) the first cumulant Γ_1 can be obtained. Since the correlation function deviates from a single exponential, second- and third-order cumulant fits were applied. Under the applied routine conditions, where 80 channels are used, the third cumulant fit deviated significantly from the second-order one. This behavior is an indication that the applied procedure might not be sufficient for a correct determination of the initial slope at $t \rightarrow 0$. Therefore, we reduced the number of channels down to 40, 35, 30, and 25 delay times until the second- and the third-order fits gave almost the same value for the initial slope $\Gamma = \Gamma_1$.

Table II
Translational Diffusion Coefficient D_z, Hydrodynamic Radius R_h, $\rho = R_g/R_h$, Coefficient C as Defined by Eq 7, and the Coefficients k_d and k_{f0}[22]

parameter	TA1-EPS	Gellan	xanthan	PBLG
$D_z \times 10^8$, cm²/s	3.58	4.70	1.55	6.65
R_h(exptl), nm	68.5	52.2	137.2	36.0
ρ(exptl)	1.80	3.06	2.17	2.81
C	0.17	0.09	0.22	0.19
k_d,[a] cm³/g	405	436	873	33.5
k_{f0}[b]	8.26	2.80	0.92	4.4

[a] Derived from the equation $D_c = D_{0z}(1 + k_d c)$. [b] Calculated according the equations $k_{f0} = k_f M/(N_A V_h)$, $k_f = 2A_2M - k_d + \bar{v}_2$, and $V_h = (4\pi/3)R_h^3$ ($\bar{v}_2$ the partial specific volume of polymer).

Figure 4 shows the angular and concentration dependence of the apparent diffusion coefficient

$$D_{app}(q) = (\Gamma_1/q^2) \quad (4)$$

in the form of a dynamic Zimm plot. Extrapolation of the apparent diffusion coefficient toward $q^2 = 0$ and $c = 0$ gives the translational diffusion coefficient D_z. Applying the Stokes–Einstein relationship

$$R_h = kT/6\pi\eta_0 D_z \quad (5)$$

the hydrodynamic radius R_h of the macromolecules can be estimated. Results are listed in Table II.

In combination with static light scattering we can acquire two further structure-sensitive dependent parameters:

(1) The first one is the ρ-parameter,[20b] which is obtained from the ratio of the geometric to hydrodynamic radius

$$\rho = R_g/R_h \quad (6)$$

(2) The second parameter is the coefficient C.[21] It is obtained from the initial slope of the angular dependence for the apparent diffusion coefficient, which is given by the equation

$$D_{app}(q) = D_c(1 + C_c\langle S^2 \rangle_c q^2 - \ldots) \quad (7)$$

At concentration c the zero-angle diffusion coefficient D_c is found from the intercept of the *dynamic* Zimm plot and the corresponding $\langle S^2 \rangle_c$ from the angular dependence of

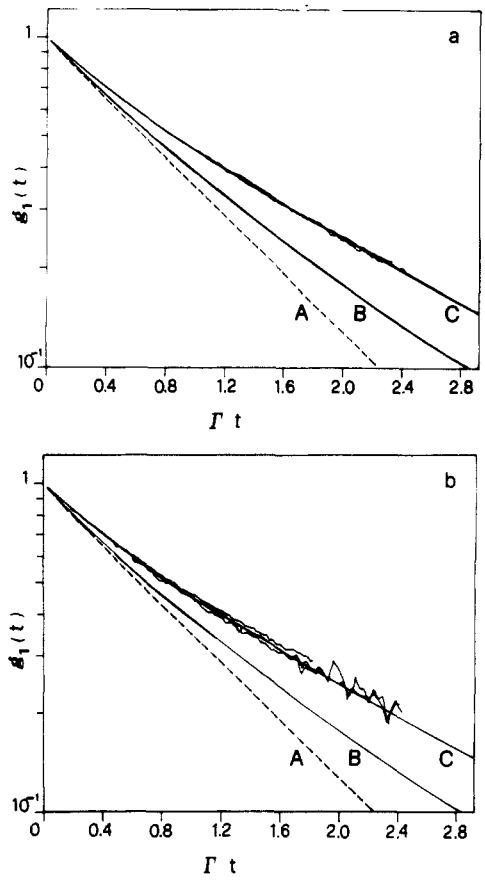

Figure 5. Shape function (=scaled time correlation function $g_1(\Gamma_t)$) (a) for TA-1-EPS in 0.1 M NaCl at $c = 2.2 \times 10^{-4}$ g/cm^3 and at scattering angles of 50°, 70°, 90°, 110°, and 130° and (b) for Gellan in 0.075 M TMACl at $c = 2.0 \times 10^{-4}$ g/cm^3 and at scattering angles of 60°, 90°, and 120°. (A) Single exponential; (B) shape function of a rod; (C) shape function of a flexible chain.

the *static* light scattering. Extrapolating the data of C_c toward $c = 0$ the parameter C is found. The two parameters, ρ and C, are given in Table II. The curvature in the angular dependence results from the spectrum of internal modes of motion, which are different for flexible and semiflexible chains.

The influence of the relaxation spectrum gives rise to a special shape of the TCF which shows characteristic scaling behavior. This "shape" function is attained from the TCFs measured at different angles by plotting them against $\Gamma_1 t$ where Γ_1 is the first cumulant. Both the TCF and the first cumulant are strongly angular dependent, but in this scaled plot the various TCFs form one common line; i.e., the whole angular dependence is absorbed in the first cumulant. The shape function has been calculated for flexible chains[23,24] with and without hydrodynamic interactions and for rigid rods.[25,26] Figure 5a shows the experimentally found shape function in comparison to the theoretically derived ones for rigid rods and flexible chains with hydrodynamic interaction.

Gellan. 1. Static Light Scattering. The counterion in this case is tetramethylammonium [$(CH_3)_4N^+$, TMA]. This ion is considerably larger than Na^+ and in addition partly hydrophobic. The Gellan sample originally in the Na form was transformed to this specific TMA form whereby polymer aggregation can be widely prevented. An ionic strength of 0.075 M TMACl was used, and under these conditions Gellan is in its ordered (helical) form in solution.[4,5]

Figure 6 shows the Zimm plot and Figure 7 the corresponding Holtzer plot for this Gellan sample. The highest

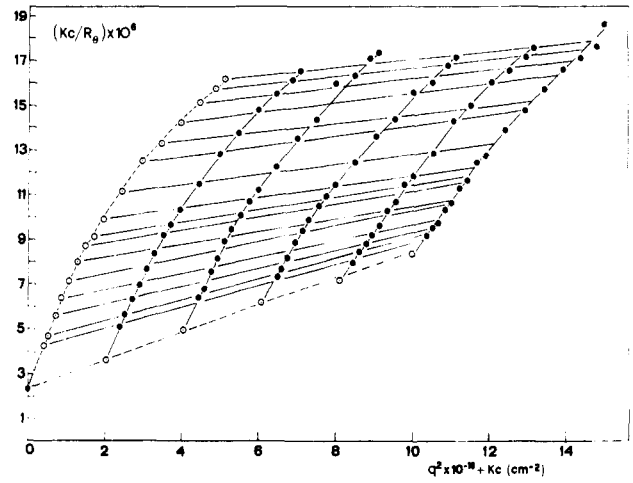

Figure 6. Zimm plot of the static light scattering measurements from Gellan in 0.075 M TMACl at 25 °C, $c = 0.20$, 0.41, 0.68, 0.81, and 1.01×10^{-3} g/cm^3.

concentration was 1.0×10^{-3} g/cm^3, which corresponds to the range of concentrations used for TA-1-EPS. Gellan has a larger radius of gyration; therefore, a wider range of $u = R_g q$ values is covered and a clear plateau is reached. The maximum position occurs at a value of 1.65, which is very near to the position for polydisperse chain at 1.73. The two diagrams were evaluated in the same manner as described in the previous section. The data are collected in Table I.

2. Dynamic Light Scattering. The dynamic Zimm plot for the apparent diffusion coefficent shown in Figure 8 has a similar appearance as for TA-1-EPS. The initial linear part at low q^2 values is better developed for Gellan than for TA-1-EPS and thus allows a more accurate determination of the coefficient C. The high accuracy can be recognized also from Figure 9 where the concentration dependence of the apparent coefficient C_c is plotted against c for the two polysaccharides. The results from dynamic measurements are given in Table II.

The shape function derived from the time correlation functions at various angles is shown in Figure 5b.

Discussion

In spite of the great difference in the primary structure of several microbial polysaccharides which have been discovered in recent years, all these chains show similar dilute solution properties. Most striking probably is the high viscosity at low concentrations, and from the present measurements and the results obtained with xanthan[9] and schizophyllan,[28] we know now that these properties are caused by an extraordinarily high chain stiffness. In fact, optical rotation measurements have shown that under the conditions applied for the present ligth scattering experiments the polysaccharides are in the ordered, i.e., helical, state.[5] In some respects ORD and LS appear to be equivalent techniques, but ORD cannot give information on the number of strands involved in such helices. Because of the very high chain stiffness the Kuhn segment length is already of the order of the wavelength of the light and this allows the study of the structure of the rodlike Kuhn segment in more detail. One property of great value is the height of the asymptotic plateau in the Holtzer plot.

Table I contains the values of the experimentally observed mass per unit length, calculated from the height of the asymptote according to eq 1. For Gellan the corresponding value of a single helix could be calculated from recent X-ray diffraction measurements by Chandrasekaran et al.[29a] From their detailed analysis the authors came to

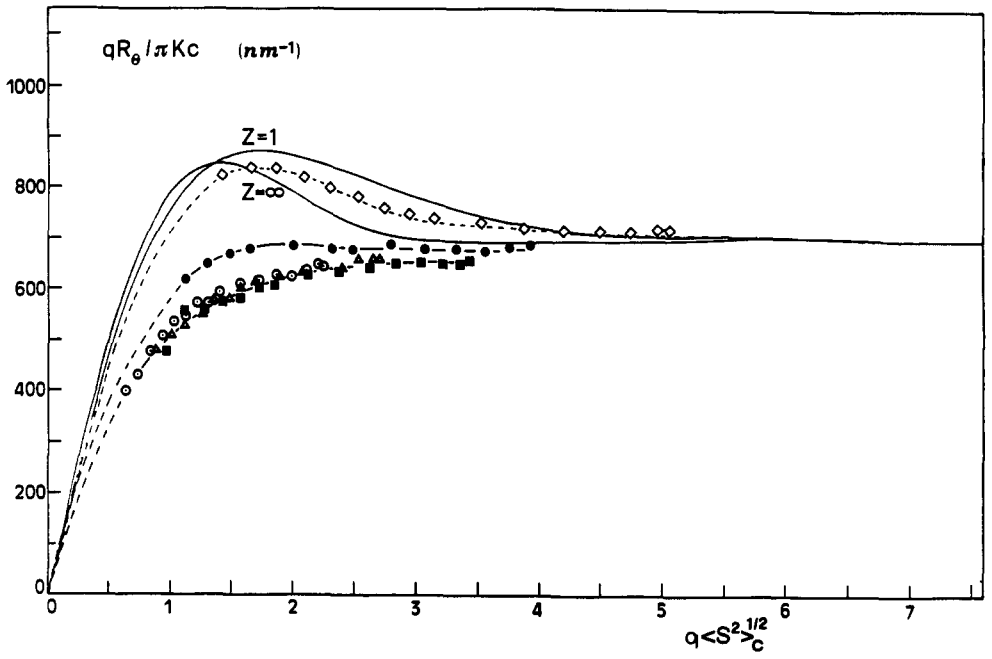

Figure 7. Holtzer plots for the same Gellan concentrations as in Figure 6 in 0.075 M TMACl at 25 °C; lowest curve corresponds to $c = 1.01 \times 10^{-3}$ g/cm^3; (◇) extrapolated values for $c = 0$; full lines were calculated according to the Koyama theory with the set of parameters as given in Table I.

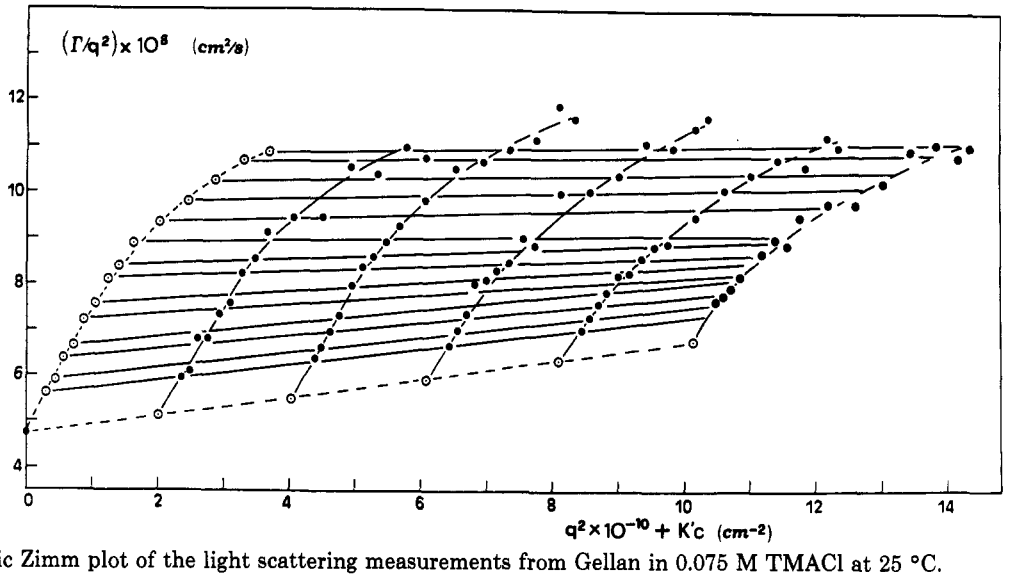

Figure 8. Dynamic Zimm plot of the light scattering measurements from Gellan in 0.075 M TMACl at 25 °C.

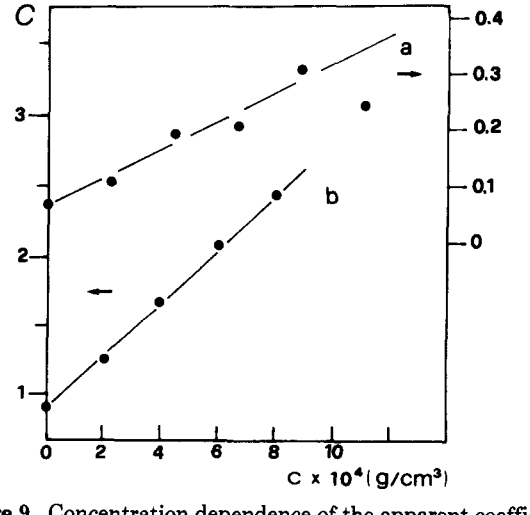

Figure 9. Concentration dependence of the apparent coefficient C in the equation $D_c(q) = D_c(1 + C\langle S^2\rangle_c q^2 - \ldots)$ for the two polysaccharides (a) TA-1-EPS and (b) Gellan.

the conclusion that Gellan forms a 3-fold intertwined double helix. The pitch, formed by three repeating units, has a value of $P = 5.64$ nm. Thus the repeating unit projected length is $l_0 = 1.88$ nm; their molecular weight is $M_0 = 720$, and thus the linear mass density of a single helix is M_L(single) = 383. Accordingly the Gellan macromolecule is built up of $n = M_L(\text{exptl})/M_L(\text{single}) = 1.85$ strands. This stands in very satisfactory agreement with the X-ray data by Chandradekaran et al.[29a]

For TA-1-EPS only estimates can be made, since X-ray data similar to those for Gellan are still missing. We assumed a projected length of $l_0 = 1.88$ nm for the four sugars in the repeating unit of the backbone. The molecular weight of the repeating unit is $M_0 = 1554$, which yields the value of M_L(single) = 827. Thus with the experimental value M_L(exptl) one finds $n = 3.02$. Thus the ordered conformation of TA-1-EPS in solution is composed of three strands.

TA-1-EPS does not form gels, and this behavior may be caused by the highly organized aggregation of the three

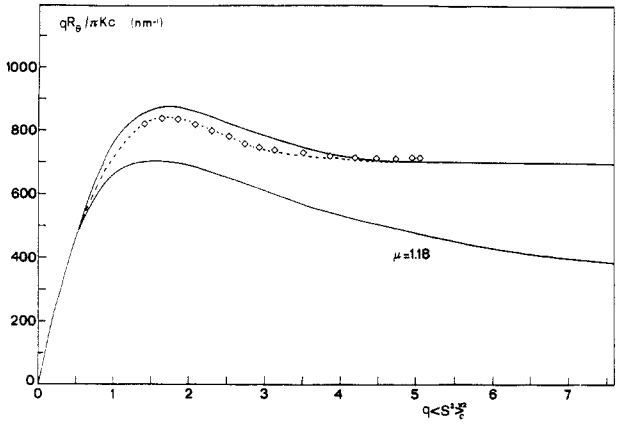

Figure 10. Holtzer plots for the scattering behavior of semiflexible chains, with the molecular data of Gellan as given in Table I, according to the Koyama theory,[18] and of a flexible chain, with large excluded volume (μ = 1.18) and the same radius of gyration and degree of polymerization, according to the theory by Loucheux et al.;[31] (◇) experimental data.

strands. The mechanism may be such that the sites, responsible for association, become saturated, possibly in a similar manner as in tropocollagen,[30] but we are not able to decide whether a real triple helix is formed; the three-stranded structure may alternatively be produced by lateral aggregation of single helices.

The value of l_0 = 1.88 nm for TA-1-EPS is of course a little arbitrary, but it appears worth mentioning here that the same length is found for xanthan and for Gellan. The values for the contour lengths L_w, the Kuhn segment lengths l_k, and the number of these segments N_k per chain given in Table I follow then from eq 2 and 3.

At this point of the discussion one may wonder whether a similar scattering curve, in the presentation of a Holtzer plot, is also obtained by excluded-volume effects. The corresponding scattering curve has been calculated independently by Ptitsyn[31a] and by Benoit and his co-workers[31b] 30 years ago. We applied the equations for monodisperse and polydisperse chains which were given by Loucheux et al. and used an exponent of $\mu = 1/\epsilon = 1.18$. The maximum excluded-volume effect corresponds to μ = 1.20, as was predicted first by Flory[32] and which now is generally used in scaling theory.[33]

The result is plotted for Gellan in Figure 10 together with the experimental data and the curve derived from Koyama's theory.[18] Clearly a chain that is expanded by excluded volume can by no means describe the experimental curve, while the Koyama theory gives a good fit. Of course, excluded volume is present in these chains ($A_2 > 0$), but its influence effects the chain conformation only if chain sections are close enough to interact. This can happen if a chain is much longer than one Kuhn segment in length. Therefore, the excluded-volume effect for such stiff chains may be observable at very small u values (i.e., for long chain section) but has no influence at large $u = qR_g$, which corresponds to chain sections of the order of one Kuhn segment.

The next point of interest is the fact that all the microbial polysaccharides have approximately the same Kuhn segment lengths, and these lengths are of the same order as those observed for the ordered polypeptides (Table III). There is a big gap in the properties of these polysaccharide chains with high Kuhn lengths and common synthetic polymers.[34] There are only a few synthetic chains known which have Kuhn lengths between 20 and 80 nm.[35-38] DNA[39] shows a strong variation of its Kuhn segment length as a function of ionic strength. This effect is induced by the electrostatic interaction which causes the chain to stretch out. A similar effect is not observed with most ionic polysaccharides in their ordered conformation. The reason for this behavior results from the comparatively low charge density in the polysaccharides and from the fact that the charges are positioned at fairly large distance along the chain. This distance is mostly larger than the Debye screening length at the applied ionic strengths. A slight increase in l_k is found, however, for TA-1-EPS at low ionic strength.[40]

Table III
Comparison of the Kuhn Segment Length l_k and Number of Associated Strands n (strands) of TA-1-EPS and Gellan with Other Biopolymers

polymer	l_k	n(strands)	ref
TA1-EPS	152[a]	3	
Gellan	322[a]	2	
xanthan	255[b]	2	9
schizophillan	390	3	28
collagen	260	3	30
PBLG	140	1	21a
DNA	120	2	39

[a] Average value for a polydispersity of M_w/M_n = 1.5. [b] Polydispersity M_w/M_n = 2.

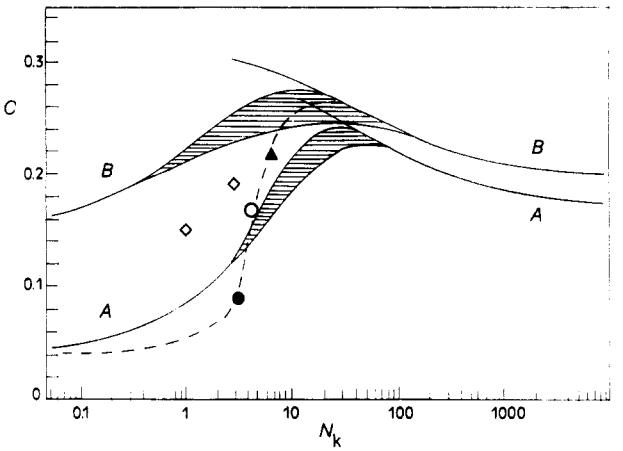

Figure 11. Experimental data for the quantity C plotted against N_k for (○) TA-1-EPS, (●) Gellan, (▲) xanthan, and (◇) PBLG at two different molecular weights. For comparison the theoretical curves for $L_w/d = 10^6$ are given: (A) monodisperse ($z = \infty$); (B) Schulz-Flory distribution (z = 1). The full curves were calculated by employing the approximations for the stiff and the flexible chain limits, respectively.[21a] The shaded area represent the Schmidt estimate for an interpolation between the two approaches.

Conclusions on chain stiffness are mostly drawn from static light scattering data, and this raises the question of whether these conclusions can be confirmed by dynamic light scattering measurements. As is shown by Schmidt and Stockmayer[21] the two parameters and C, defined by eq 6 and 7, should give additional information on chain stiffness. The variation of these parameters with the number of Kuhn segments according to their estimation is shown in Figures 11 and 12. These figures also contain the experimental data for the three polysaccharides of Table II and two points for PBLG as measured by Schmidt.[21a] The ρ values for the polysaccharides are consistent with the values observed for PBLG by Schmidt, and they show the correct dependence on the number of Kuhn segments. The experimental data would correspond to chains with large cross-section diameters. The cross section can be estimated from the linear mass density M_L and the partial specific volume $\bar{v}$

$$\bar{v} = (\pi N_A/4)(d^2/M_L) \quad (8)$$

Assuming $\bar{v}$ = 0.68 for the polysaccharides, one obtains with the data of Table I $d \cong 1.89$ nm (TA1-ESP), $d \cong 1.01$

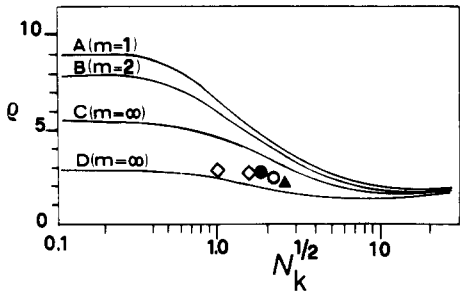

Figure 12. Experimental data for the parameter versus $N_k^{1/2}$ for (○) TA-1-EPS, (●) Gellan, (▲) xanthan, and (◇) PBLG at two different molecular weights. For comparison the parameter ρ calculated by Schmidt for different polydispersities is also represented.[21a] Curves A–C: $L_w/d = 10^4$. Curve D: $L_w/d = 10^2$. $m = z$, polydispersity parameter; $z = 1$, $M_w/M_n = 2$; $z = M_w/M_n = 1.5$; $z = \infty$, $M_w/M_n = 1$.

nm (Gellan), and $d \cong 1.62$ nm (xanthan). These data represent lower bounds. The hydrodynamically effective radii may be larger since the side chains may stretch out orthogonally to the backbone.

The experimental C parameters for PLBG samples do not form a common curve with the three polysaccharides. It appears that at large numbers of Kuhn segments the correct limit for flexible chain (curve B, polydisperse chains) is approached, but for a smaller number of Kuhn segments the C parameter seems to decay much more strongly than predicted. The C parameter gives first information on the internal flexibility of the chains but it corresponds to a certain molecular average. Thus, a dependence on polydispersity and on the hydrodynamically effective chain cross-section exits. Probably, however, the following reason is most likely responsible for the deviation from theory. If a chain is very stiff the orientational fluctuations of the Kuhn segments become a very fast process which no longer can be detected by the autocorrelator. This nondetectable contribution from the rotational diffusion reduces the C parameter significantly. Therefore, of the two parameters ρ and C the ρ-value gives more reliable conclusions on structure.

Another possibility to obtain information on chain stiffness arises from the *relaxation spectrum*. This spectrum has its reflection in a special form of the TCF $g_1(\Gamma t)$. In the previous study of xanthan, a clear transition of rodlike behavior at short delay times to that of flexible chains was observed.[9] For the present two polysaccharides we find a good agreement with the shape function of flexible chains, although the two polysaccharides and xanthan have similar rigidity (parts a and b of Figure 5 for TA-1-EPS and Gellan, respectively). It appears possible that the Kuhn segments in xanthan behave like truly rigid rods; in the two other polysaccharides, on the other hand, the units in the Kuhn segment may still have some flexibility, as would befit the wormlike chain model. Polydispersity is expected to have only little effect on the shape of the time correlation function in these time- and q-domains, because this shape is here determined only by internal modes of motion and no longer by the translational diffusion coefficient, which, of course, is strongly chain length dependent.

The last point to be discussed is the angular dependence of the apparent diffusion coefficient at infinite dilution. In Figure 13 the ratio of $D_{app}(q)/D_0$ for TA-1-EPS, Gellan, and for native xanthan is plotted against the dimensionless parameter qL. The two theoretical curves for a rigid-rod and for the sliding-rod model do not describe the measurements. It is, however, instructive to calculate the ratio $D_\infty(\text{segment})/D_0$) at very large q values, assuming the

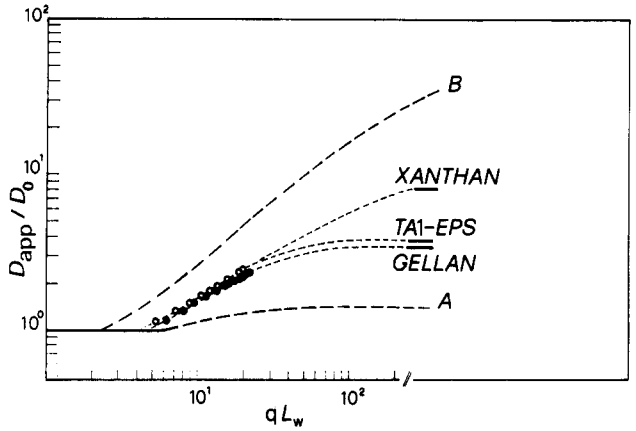

Figure 13. Normalized apparent diffusion coefficient D_{app}/D_0 versus qL_w; D_0 is the translational diffusion coefficient at concentrations $c = 0$ and $q = 0$. (A) theoretical curve for a rigid rod[37] assuming the contour length as the rod length; B) theoretical curve for the sliding-rod model;[38] (○, ●) experimental points for TA-1-EPS and Gellan. The bars indicate the limiting plateau values according to the Hammouda theory, assuming the Kuhn length as a rod.

Kuhn segment to behave as a rigid rod. This ratio can be estimated by Hammouda's theory:[41]

$$D_\infty(\text{segment})/D_0 = 1.5 \ln (l_k/d)(2R_h/l_k)$$

where d is the chain diameter. The data are indicated by bars on the right side of Figure 13.

It is not surprising that the theoretical curves A and B do not describe the experiment: the present polysaccharides are not completely rigid; on the other hand it has been pointed out by Hammouda[41] that the sliding-rod model[42] is capable of describing only chains of rather high flexibility. Evidently these polysaccharides are more rigid than in the corresponding sliding-rod model. The experimental curves appear to lead into the asymptote of a rod whose length is that of a Kuhn segment, which is a sensible behavior of the wormlike chain model. We have to mention, however, that the asymptotic values depend not solely on the chain stiffness but also on the dimensional chain thickness as can be recognized from eq 9. Also, the right-hand side in eq 9 refers to the apparent segment diffusion at $q = 0$ (D_0) and $q \gg 1$ (D_∞), whereas the experimental D_0 is the translational diffusion coefficient of the wormlike chain and D_∞ that of a Kuhn segment at very large q values. Thus the asymptotic values of eq 9 will in general not coincide with the experimental asymptote.

Acknowledgment. We are grateful to Dr. Manfred Schmidt, Max Planck Institut für Polymerforschung, Mainz, for helpful discussions. The project was supported by the Deutsche Forschungsgemeinschaft within the scheme SFB 60.

Registry No. Gellan, 85087-30-5.

References and Notes

(1) Kenne, L.; Lindberg, B. In *The Polysaccharides*; Aspinall, G. O., Ed.; Academic: New York, 1983; Vol. 2, p 287.
(2) Sandford, P. A.; Baird, J. In *The Polysaccharides*; Aspinall, G. O., Ed.; Academic: New York, 1983; Vol. 2, p 412.
(3) Crescenzi, V.; Dentini, M.; Coviello, T. In *Recent Developments in Industrial Polysaccharides*; Stivala, S. S., Crescenzi, V., Dea, I. M. M., Eds.; Gordon & Breach: New York, 1987; p 68.
(4) Crescenzi, V.; Dentini, M.; Coviello, T.; Rizzo, R. *Carbohydr. Res.* **1986**, *149*, 425.
(5) Crescenzi, V.; Dentini, M.; Dea, I. C. M. *Carbohydr. Res.* **1987**, *160*, 283.
(6) Norton, I. T.; Goodall, E. R.; Morris, E. R.; Rees, D. A. *J. Chem. Soc., Chem. Commun.* **1979**, 988.

(7) Norton, I. T.; Goodall, E. R.; Morris, E. R.; Rees, D. A. *J. Chem. Soc., Chem. Commun.* **1980**, 545.
(8) Dentini, M.; Crescenzi, V.; Blasi, D. *Int. J. Biol. Macromol.* **1984**, *6*, 93.
(9) Coviello, T.; Kajiwara, K.; Burchard, W.; Dentini, M.; Creszenzi, V. *Macromolecules* **1986**, *19*, 2826.
(10) Coviello, T.; Burchard, W.; Dentini, M.; Crescenci, V. *Macromolecules* **1987**, *20*, 1102.
(11) Crescenzi, V.; Dentini, M.; Coviello, T.; Paoletti, S.; Cesaro, A.; Delben, F. *Gazz. Chim. Ital.*, in press.
(12) Zevenhuizen, L. P. T. M.; Van Nerven, A. R. W. *Carbohydr. Res.* **1983**, *124*, 166.
(13) Bantle, S.; Schimdt, M.; Burchard, W. *Macromolecules* **1982**, *15*, 1604.
(14) Burchard, W. In *Applied Fibre Science*; Happey, F., Ed.; Academic: London, 1978; p 381.
(15) Kratochvil, P. In *Light Scattering from Polymer Solutions*; Huglin, M. B., Ed.; Academic: London, 1972; p 333.
(16) Schmidt, M.; Paradossi, G.; Burchard, W. *Makromol. Chem. Rapid Commun.* **1985**, *6*, 767.
(17) (a) Holtzer, A. J. *J. Polym. Sci.* **1955**, *17*, 432. (b) Casassa, E. F.; Eisenberg, H. *Adv. Protein Chem.* **1964**.
(18) Koyama, R. *J. Phys. Soc. Jpn.* **1973**, *34*, 1029.
(19) Benoit, H.; Doty, P. J. *J. Phys. Chem.* **1953**, *57*, 958.
(20) (a) Burchard, W.; Schmidt, M.; Stockmayer, W. H. *Macromolecules* **1980**, *13*, 580. (b) Burchard, W.; Schmidt, M.; Stockmayer, W. H. *Macromolecules* **1980**, *13*, 1265.
(21) (a) Schmidt, M. *Macromolecules* **1984**, *17*, 553. (b) Schmidt, M.; Stockmayer, W. H. *Macromolecules* **1984**, *17*, 509.
(22) (a) Pyun, C. W.; Fixman, M. *J. Chem. Phys.* **1964**, *41*, 937. (b) Yamakawa, H.; *Modern Theory of Polymer Solutions*; Harper & Row: New York, 1971.
(23) (a) de Gennes, P.-G. *Physics (Long Island City, N.Y.)* **1967**, *3*, 37. (b) de Gennes, P.-G.; Dubois-Violette *Physics Long Island City, N.Y.)* **1967**, *3*, 181.
(24) Akasu, A. Z.; Benmouna, M.; Han, C. C. *Polymer* **1980**, *20*, 866.
(25) Hallet, F. R.; Nickel, B.; Craig, T. *Biopolymers* **1985**, *24*, 947.
(26) (a) Wilcoxon, J.; Schurr, J. M. *Biopolymer* **1983**, *22*, 849. (b) Maeda, T.; Fujime, S. *Macromolecules* **1984**, *17*, 1157.
(27) Paradossi, G.; Brant, D. A. *Macromolecules* **1982**, *15*, 874.
(28) Yanaki, T.; Norisuye, T.; Fujita, H. *Macromolecules* **1980**, *13*, 1462.
(29) (a) Chandrasekaran, R.; Millane, R. P.; Arnott, S.; Atkins, E. D. T. *Carbohydr. Res.* **1987**, 160. (b) Upstill, G.; Atkins, E. D. T.; Attwool, P. T. *Int. J. Biol. Macromol.* **1986**, *8*, 275.
(30) Utiyama, H.; Sakato, K.; Ikehara, K.; Setsuiye, T.; Kurata, M. *Biopolymers* **1974**, *12*, 53.
(31) (a) Ptitsyn, O. B. *Zh. Fiz. Khim.* **1957**, *31*, 1091. (b) Loucheux, C.; Weill, G.; Benoit, H. *J. Chim. Phys. Phys.-Chim Biol.* **1958**, *55*, 540.
(32) Flory, P. J. *Principles of Polymer Chemistry*; Cornell University: Ithaca, 1953; Chapter 14.
(33) de Gennes, P.-G. *Scaling Concepts in Polymer Physics*; Cornell University: Ithaca, 1979.
(34) Brandrup, J., Immergut, E. H., Eds. *Polymer Handbook*; Interscience: New York, 1966.
(35) Murakami, H.; Norisuye, T.; Fujita, H. *Macromolecules* **1980**, *13*, 345.
(36) Berry, G. C. In *Contemporary Topics in Polymer Science*; Pearce, E. M., Schaefgen, J. R., Eds.; Plenum: New York, 1977; Vol. 2.
(37) Strazielle, C.; Arpin, M. *Makromol. Chem.* **1976**, *177*, 581.
(38) Ying, Q.; Chu, B. *Makromol. Chemie, Rapid Commun.* **1984**, *5*, 785.
(39) (a) Godfrey, J. E.; Eisenberg, H. *Biophys. Chem.* **1976**, *5*, 30. (b) Borochov, N.; Eisenberg, H. *Biopolymers* **1984**, *23*, 1757.
(40) Coviello, T.; et al., submitted for publication.
(41) Hammouda, B. *Macromolecules* **1985**, *18*, 293.
(42) Benmouna, M.; Akcasu, A. Z.; Daoud, M. *Macromolecules* **1980**, *13*, 1703.

Behavior of $\langle r^2\mu^2\rangle_0$ in Several Monosubstituted Vinyl Polymers

Wayne L. Mattice

Institute of Polymer Science, The University of Akron, Akron, Ohio 44325.
Received February 19, 1988; Revised Manuscript Received April 15, 1988

ABSTRACT: Generator matrix methods have been used to compute $\langle r^2\mu^2\rangle_0$, $\langle r^2\rangle_0$, and $\langle \mu^2\rangle_0$ for poly(vinyl bromide), poly(vinyl chloride), and poly(styrene) chains as functions of the stereochemical composition. The squared end-to-end distance and squared dipole moment are denoted by r^2 and μ^2, respectively, angle brackets denote the statistical mechanical average of the enclosed property, and zero as a subscript denotes the ensemble that is unperturbed by long-range interactions. The values of $\langle r^2\mu^2\rangle_0/\langle r^2\rangle_0\langle \mu^2\rangle_0$ are larger than 1 for chains with a finite number of bonds, n. They approach 1 as a limit as n increases. At a specified value of n, the largest values of $\langle r^2\mu^2\rangle_0/\langle r^2\rangle_0\langle \mu^2\rangle_0$ are obtained with racemic poly(vinyl chloride) chains. The tendency for a correlation of μ^2 with r^2 arises from the parallel alignment of the components of the C–Cl bond in the plane of the backbone atoms in the fully extended racemic chain. Simulations that permit the introduction of excluded volume show that $\langle \mu^2\rangle$ for all three chains is insensitive to $\langle r^2\rangle/\langle r^2\rangle_0$ unless the stereochemical composition is predominantly racemic. The response of $\langle \mu^2\rangle$ to chain expansion is more dramatic in racemic poly(vinyl chloride) than in the other two polymers.

The mean-square end-to-end distance, $\langle r^2\rangle$, is sufficient for the specification of the distribution function, $W(\mathbf{r})$, for the end-to-end vector, $\mathbf{r}$, in the special case where that distribution function is Gaussian. Expressions for $W(\mathbf{r})$ that more accurately describe the distribution function for real chains are available. A common approach is formulation of $W(\mathbf{r})$ in terms of the higher even moments of $\mathbf{r}$. In the formulation due to Nagai,[1] departures from a Gaussian distribution function are expressed by a series of terms that contain dimensionless ratios of the form $\langle r^{2\nu}\rangle/\langle r^2\rangle^{\nu}$. Deviation of the values of the dimensionless ratios from their asymptotic limits at large n is seen in chains of finite n. For example, $\langle r^4\rangle_0/\langle r^2\rangle_0^2$ and $\langle r^6\rangle_0/\langle r^2\rangle_0^3$ are less than $^5/_3$ and $^{35}/_9$, respectively, for unperturbed polyethylene chains with finite n, but they approach the Gaussian limits of $^5/_3$ and $^{35}/_9$ as n becomes infinite.[2] Nagai's formulation uses the actual values of $\langle r^{2\nu}\rangle/\langle r^2\rangle^{\nu}$ to increase the accuracy of the expression for $W(\mathbf{r})$.

Methodology is available for the efficient computation of $\langle r^4\rangle_0/\langle r^2\rangle_0^2$ for real unperturbed chains via the rotational isomeric state theory. The method derives from the expression of r^4 for a specified conformation as $r^2 \otimes r^2$ (where $\otimes$ denotes the direct product) and an appeal to the theorem on direct products.[3] The averaging over all conformation accessible to the unperturbed chain is obtained by the usual combination of statistical weight matrices and generator matrices that contain information about the

0024-9297/88/2221-3320$01.50/0